Bioorganic Chemistry 93 (2019) 103327

Contents lists available at ScienceDirect

Bioorganic Chemistry

journal homepage: www.elsevier.com/locate/bioorg

Novel triazole-tetrahydroisoquinoline hybrids as human aromatase inhibitors

Chanamon Chamduang[a], Ratchanok Pingaew[a,*], Veda Prachayasittikul[b,*], Supaluk Prachayasittikul[b], Somsak Ruchirawat[c,d], Virapong Prachayasittikul[e]

[a] Department of Chemistry, Faculty of Science, Srinakharinwirot University, Bangkok 10110, Thailand
[b] Center of Data Mining and Biomedical Informatics, Faculty of Medical Technology, Mahidol University, Bangkok 10700, Thailand
[c] Laboratory of Medicinal Chemistry, Chulabhorn Research Institute, and Program in Chemical Biology, Chulabhorn Graduate Institute, Bangkok 10210, Thailand
[d] Center of Excellence on Environmental Health and Toxicology, Commission on Higher, Education (CHE), Ministry of Education, Thailand
[e] Department of Clinical Microbiology and Applied Technology, Faculty of Medical Technology, Mahidol University, Bangkok 10700, Thailand

ARTICLE INFO

Keywords:
Triazole
Isoquinoline
Sulfonamide
Synthesis
Aromatase inhibitor
Molecular docking

ABSTRACT

Novel thirteen triazole-tetrahydroisoquinoline derivatives (**2a-m**) were synthesized and evaluated for their aromatase inhibitory activities. Seven triazoles showed significant aromatase inhibitory activity (IC_{50} = 0.07–1.9 μM). Interestingly, the analog bearing naphthalenyloxymethyl substituent at position 4 of the triazole ring (**2i**) displayed the most potent aromatase inhibitory activity (IC_{50} = 70 nM) without significant cytotoxicity to a normal cell. Molecular docking also suggested that the direct H-bonding interaction with residue Thr310 may be responsible for a striking inhibitory effect of the most potent compound **2i**.

1. Introduction

High level of estrogen has been noted to promote cancer cell growth, recurrence, and metastasis of the estrogen-dependent breast cancers. Regardingly, decreasing estrogen level by inhibiting its biosynthesis is considered to be one of the effective strategies for breast cancer management [1–7]. Aromatase (CYP19), a member of the cytochrome P450 family, is a rate-limiting enzyme that catalyzes the biosynthesis of estrogens from androgens. Therefore, aromatase inhibitors (AIs) have been recognized as one of the widely used drug classes for management of estrogen-dependent cancer [1–7]. AIs are categorized by their mechanisms of action into two main types: (i) steroidal AIs (such as formestane and exemestane) which irreversibly inhibit activity of the aromatase enzyme, and (ii) nonsteroidal AIs (such as letrozole, anastrozole, and vorozole) which their inhibitory effects are reversible (Fig. 1) [3–7]. Although available aromatase inhibitors (both steroidal and non-steroidal types) displayed successful clinical outcomes, long-term use can lead to acquired drug resistane as well as considerable side effects including musculoskeletal pain, osteoporosis, broken bones, and cardiovascular disease [8–11]. Therefore, development of novel aromatase inhibitors is still essential to provide alternative drug of choice with more preferable properties.

Triazoles are core structure regularly found in nonsteroidal AIs [2,3,5,7]. Among the classes of AI (Fig. 1), letrozole and anastrozole containing triazole ring were approved by the United States Food and Drug Administration (FDA) for the treatment of advanced breast cancer in postmenopausal women [12]. The heterocyclic nitrogen atom of triazole plays an important role by interacting with the heme iron of the aromatase enzyme [3,6,7]. Along the line, the aromatase inhibitory activity of a series of 1,2,3-triazoles bearing sulfonamide has been reported by our group (Fig. 2) [13]. The study revealed that various tested triazoles displayed significant inhibitory potency with IC_{50} ranging from 0.2 to 9.4 μM, where the tetrahydroisoquinoline-triazole (THIQ-triazole) **1** was shown to be the most potent inhibitor. The molecular docking results of the triazole **1** against the aromatase disclosed the crucial interactions namely hydrophobic interaction using THIQ and benzene rings; π-π stacking interaction using triazole and coumarinyl rings; and hydrogen bond interaction using sulfonyl and ether groups. In our previous work, the sulfonamide moiety plays crucial role in H-bond formation with His480 of the enzyme giving rise to potent aromatase inhibitory effect of the compounds [14]. Therefore, as inspired by the parent compound **1**, a series of novel THIQ-triazole **2** was modified (Fig. 2). Accordingly, THIQ-SO_2-benzene-triazole core of the hit compound **1** was preserved to remain the hydrophobic, π-π stacking, and H-bonding interactions with the enzyme, but the oxymethylcoumarinyl moiety was replaced with different hydrophobic

* Corresponding authors.
E-mail addresses: ratchanok@swu.ac.th (R. Pingaew), veda.pra@mahidol.ac.th (V. Prachayasittikul).

https://doi.org/10.1016/j.bioorg.2019.103327
Received 23 April 2019; Received in revised form 14 August 2019; Accepted 27 September 2019
Available online 28 September 2019

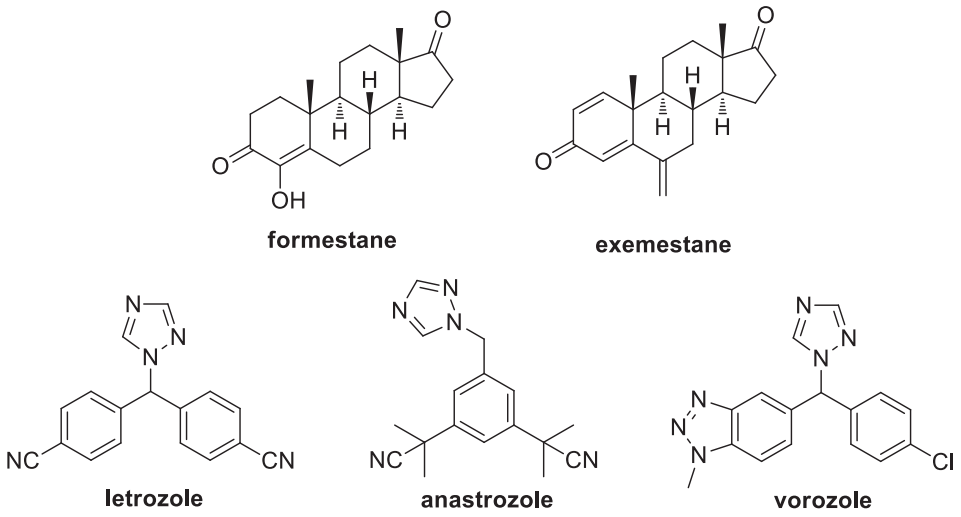

Fig. 1. Representative aromatase inhibitors.

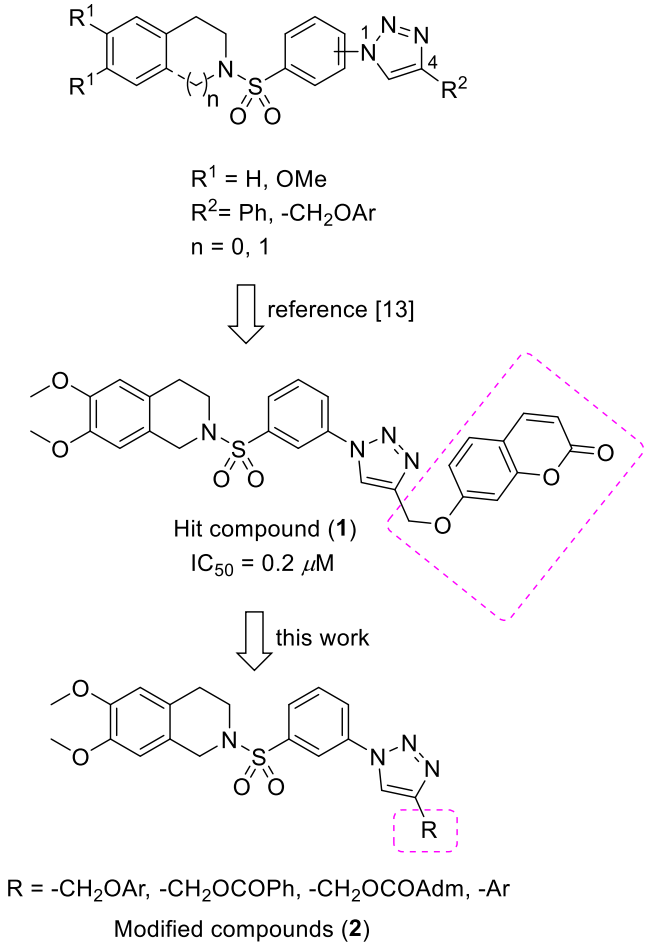

Fig. 2. Aromatase inhibitors containing triazole; hit compound (1) and modified compounds (**2**).

groups (R) to attain an optimal interaction with the target.

All of the novel synthesized triazole derivatives were evaluated for their aromatase inhibitory activities. To provide insights into the important interactions, the molecular docking study was also performed to investigate possible binding modes governing the aromatase inhibitory activities.

2. Results and discussion

2.1. Chemistry

Alkynes **5a-k** were prepared by alkylation reaction of the corresponding phenols or carboxylic acids **3a-k** with propargyl bromide using K_2CO_3 as a base in acetone or in DMF, whereas alkynes **5l** and **5m** were procured from the commercially available sources. 2-((3-Azidophenyl)sulfonyl)-6,7-dimethoxy-1,2,3,4-tetrahydroisoquinoline **6** has been prepared according to the method reported by our group [13]. The copper(I)-catalyzed alkyne-azide cycloaddition (CuAAC) of the azide **6** and alkynes **5** was performed to afford the desired 1,2,3-triazole products **2a-m** in good yields (70–94%) (see Scheme 1).

Structures of the novel 1,2,3-triazoles **2** were well characterized by their ^{1}H NMR, ^{13}C NMR, HRMS and IR spectra. ^{1}H NMR of all products showed a singlet peak with down field chemical shift at δ in the range of 8.10–8.32 ppm, which indicated that the triazole ring was formed, and HRMS data were in accordance with the expected chemical structures. In case of derivatives **2j** and **2k**, their carbonyl carbons (CO) were observed at δ 166.6 and 177.6 ppm, respectively in ^{13}C NMR spectra, and their vibration absorption bands (IR spectra) of C=O groups appeared at 1717 and 1724 cm^{-1}, respectively.

2.2. Biological activity

2.2.1. Aromatase inhibitory activity and Structure-activity relationships (SAR)

The novel thirteen isoquinoline-sulfonamide-triazole derivatives (**2a-m**) with different substituents (R) at position 4 of the triazole core, were assayed for their aromatase inhibitory activities. The derivatives (**2a**, **2e-h** and **2m**) with the inhibition ≤50% were identified as inactive compound (IC_{50} > 12.5 μM), and the compounds (**2b-d** and **2i-l**) with inhibition > 50% were further evaluated for their IC_{50} values using ketoconazole and letrozole as the reference drugs as shown in Table 1.

Seven derivatives (**2b-d** and **2i-l**) displayed the aromatase inhibitory activity better than the ketoconazole, but lesser than the letrozole. The study indicated that hydrophobic substituents (R) on the triazole ring play important roles in governing their aromatase inhibitory activities, and a structure–activity relationship (SAR) of the tested compounds is discussed. No significant inhibitory effect was observed for triazole **2a** bearing phenoxymethyl (R) group on the triazole ring. However, derivatives **2b-d** achieved from an introduction of lipophilic substituents (methyl, ethyl and propyl moieties) at *para*

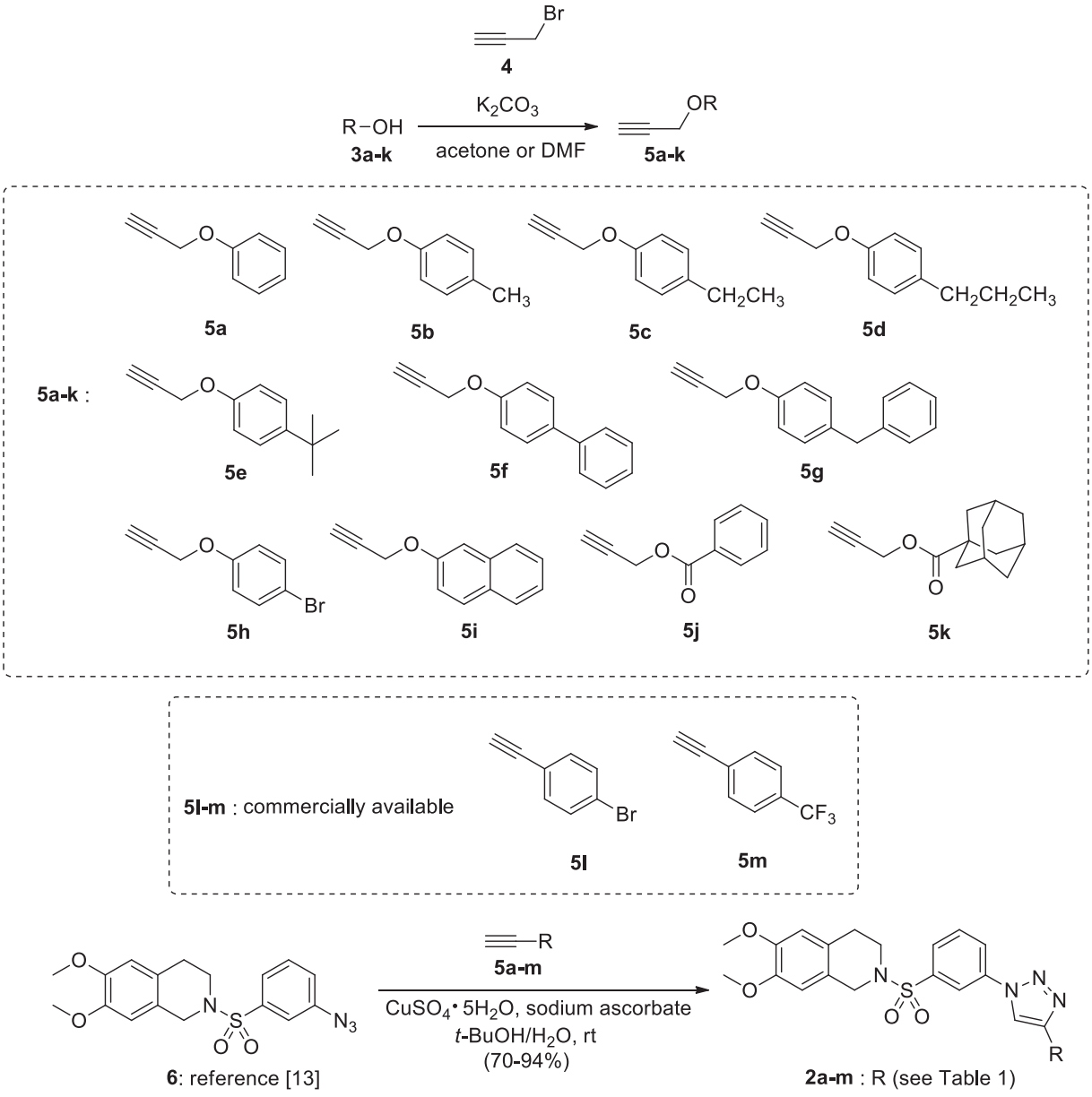

Scheme 1. Synthesis of triazole-tetrahydroisoquinoline hybrids **2a-m** through the Click reaction.

position on the oxyphenyl ring of compound **2a** displayed the inhibitory effect with IC_{50} values in the range of 0.2–1.7 μM. Apparently, the triazoles **2b** with methyl group and **2d** with propyl group had comparable IC_{50} values with that of the hit compound (**1**, IC_{50} = 0.2 μM) containing 7-coumarinyl substituent on the triazole ring [13]. Unfortunately, triazoles (**2e-h**) were shown to be inactive. The results indicated that steric bulky groups (*t*-butyl, phenyl, benzyl and bromo groups) substituted on the phenyl ring of R group hindered the crucial interaction with the target site. Because the volume of the aromatase active site is very small [15], the bulky group presented in these compounds may lead to loss of ability to reach active site and loss of the activity. When the phenyl group of compound **2a** was replaced with 2-naphthalenyl ring as found in compound **2i** (R = 2-napthalenyloxymethyl), the distinctively enhanced inhibitory potency was observed. The compound **2i** was shown to be the most active derivative (IC_{50} = 0.07 μM) with 3-fold more potent than the hit compound **1** (R = coumarinyloxymethyl) [11].

Inhibitory potency was remarkably improved as noted in ester **2j** (IC_{50} = 0.8 μM) resulting from the insertion of C═O group between O-Phenyl bond of the analog **2a** (IC_{50} > 12.5 μM). When the phenyl group of compound **2j** was replaced with 1-adamantanyl group leading to ester **2k** (IC_{50} = 1.9 μM), the observed potency was 2-fold reduction. The result implies that the phenyl ring may be required for π-π stacking and/or hydrophobic interaction with the target site. Inhibitory potency was observed when the oxymethyl group of compound **2h** (IC_{50} > 12.5 μM) was removed to give the active compound **2l** (IC_{50} = 0.6 μM). This could suggest that the bromo derivative without oxymethyl group (**2l**) might be an appropriate size required for hydrophobic interaction with the target site of action when compared with the bigger molecule containing oxymethyl moiety (**2h**). At this point, it could be hypothesized that synthesis of the most active compound **2i** without the oxymethyl moiety is attractive to be further studied. Replacement of the bromo substituent of triazole **2l** with trifluoromethyl (CF_3) substituent led to the compound **2m** with loss of the activity. It could be due to the lower lipophilic effect of CF_3 group compared with the Br group.

Table 1

Aromatase inhibitory activity and cytotoxic activity (IC_{50}, μM) of triazoles (**2a-m**).

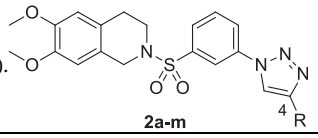

2a-m

Compound	R	Aromatase inhibitory activity	Cytotoxic activity		Selectivity index[a] (SI)
			T47-D	MRC-5	
2a	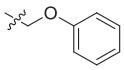	> 12.5	Non-cytotoxic	Non-cytotoxic	–
2b	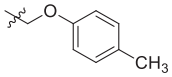	0.3 ± 0.1	22.26 ± 0.579	30.96 ± 4.978	103.21
2c	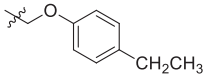	1.7 ± 0.4	14.85 ± 2.474	4.66 ± 0.473	2.74
2d	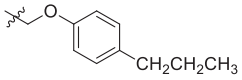	0.2 ± 0.0	26.81 ± 3.415	6.40 ± 0.586	31.99
2e	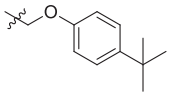	> 12.5	8.66 ± 0.424	6.43 ± 0.848	–
2f	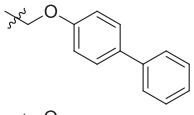	> 12.5	14.78 ± 1.209	77.68 ± 0.572	–
2g	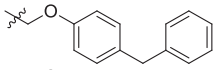	> 12.5	Non-cytotoxic	75.26 ± 2.298	–
2h	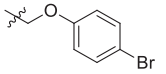	> 12.5	Non-cytotoxic	Non-cytotoxic	–
2i	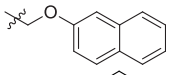	0.070 ± 0.025	58.85 ± 6.208	Non-cytotoxic	> 1283.23
2j	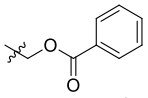	0.8 ± 0.4	Non-cytotoxic	Non-cytotoxic	> 116.91
2k	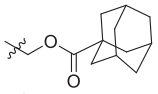	1.9 ± 0.5	Non-cytotoxic	13.28 ± 0.360	6.99
2l	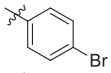	0.6 ± 0.4	Non-cytotoxic	Non-cytotoxic	> 150.03
2m	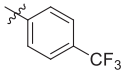	> 12.5	34.78 ± 1.032	67.10 ± 4.186	–
Ketoconazole[b]		2.6 ± 0.7	–	–	–
Letrozole[b]		0.0019 ± 0.0002	–	–	–
Etoposide[b]		–		13.35 ± 0.374	–
Doxorubicin[b]		–	0.88 ± 0.021	2.19 ± 0.37	–

T47-D = hormone-dependent breast cancer cell line; MRC-5 = normal embryonic lung cell line.
Non-cytotoxic = IC_{50} > 50 μg/mL.

[a] SI = IC_{50} for MRC-5/ IC_{50} for aromatase.

[b] Ketoconazole, letrozole, etoposide and doxorubicin were used as reference drugs.

2.2.2. Cytotoxic activity

These triazoles (**2a-m**) were further evaluated for their cytotoxic effects against the hormone-dependent breast cancer cell line (T47-D) using MTT assay (Table 1). The results showed that compounds **2b-f, 2i** and **2m** exhibited moderate cytotoxic activity (IC_{50} 8.66–58.85 μM). The compounds **2e**, **2f** and **2m** displayed cytotoxic activity against T47-D cells whereas they were shown to be inactive for aromatase inhibitory potency (IC_{50} > 12.5 μM). These could be anticipated that the potent cytotoxic effect of compounds **2e**, **2f** and **2m** may be responsible by different mechanisms and/or biological targets [16–20].

These compounds were also investigated against normal embryonic lung cells (MRC-5) using MTT assay to determine the safety index (Table 1). It was found that the active analogs (**2b-d** and **2k**) showed cytotoxicity to non-cancerous cell in the range of 4.66–30.96 μM. Interestingly, the potent analogs (**2i**, **2j** and **2l**) were non-cytotoxic toward the normal cell, and the most potent triazole **2i** had very high safety index with a selectivity index (SI) value of > 1283.

2.3. Molecular docking

Molecular docking of the investigated triazole analogs **2a-m** was performed against the target protein to reveal possible binding modes

of the compounds. Crystal structure of human placental aromatase cytochrome P450 in complex with androstenedione (PDB: 3EQM) was selected as a target protein due to its acceptably high resolution (2.9 Å) and its androgenic specificity [15]. The target protein underwent preparation processes including repairing missing side chains and adding essential hydrogen atoms followed by merging non-polar hydrogen atoms, assigning Gasteiger atomic charges, and specifying atom type of the protein structures. All investigated compounds were drawn, geometrically optimized, and prepared by defining rotatable bonds, merging non-polar hydrogen atoms, and assigning partial atomic charge. Before investigating possible binding modes of the studied compounds, the docking protocol need to be validated to ensure its performance. Redocking is one of the widely used *pose selection* validation methods, which is performed by docking a ligand with known conformation and orientation in the active site of the target, which is typically derived from a co-crystal protein structure [21]. Success of pose prediction of the docking protocol was evaluated by comparing the different between original co-crystalized position and redock position (which is calculated by root mean squared deviation: RMSD value), the docking protocol providing RMSD less than 2 Å is considered to perform successfully [22]. The validation of docking protocol was conducted by redocking the co-crystallized ligand androstenedione (ASD) to the aromatase enzyme. The redocking provided acceptable RMSD value of 0.705 Å (Fig. 3A). The same docking protocol was subsequently employed to investigate possible binding modes of the triazole derivatives (**2a-m**). The molecular docking results showed that all investigated triazole derivatives could occupy within the active site of the aromatase enzyme (Fig. 3B). Compound **2i** (IC_{50} = 0.07 μM) was selected as a representative compound for detailed discussion according to its most potent inhibitory activity (Fig. 3C). The 2D ligand-protein interaction diagrams (Fig. 4) showed that the oxygen atoms of oxymethylene linker between naphthalene and triazole rings, and of methoxyl group substituted on the isoquinoline ring of compound **2i** could form hydrogen bonding interactions with the residues Ser478 and Thr310 of the aromatase enzyme, respectively (Fig. 4B). The THIQ moiety of compound **2i** could also mimic steroidal backbone of the natural ASD by forming hydrophobic interaction with Ile133 residue (Fig. 4B). Moreover, other hydrophobic parts (naphthalenyl and benzene sulfonyl) of the compound **2i** could form hydrophobic interactions with residues Ser478, His480, Asp309, Phe221, and Val370 (Fig. 4B). In addition, the same set of enzyme residues (i.e., Ser478, Asp309, Val370, and Phe221) are involved in the hydrophobic interactions of the second most potent compound **2d**, IC_{50} = 0.2 μM (Fig. 4C), and the third most potent compound **2b**, IC_{50} = 0.3 μM (Fig. 4D). Particularly, the Phe221 displayed π-π stacking interactions with the triazole ring of these active compounds (**2i**, **2d**, and **2b**). This Phe221 residue also played role in forming π-π stacking interaction with the phenyl ring substituted at position 4 of the triazole moiety of compounds **2d**, and **2b** as well as the naphthalenyl ring substituted at position 4 of the triazole moiety of **2i**. Such π- π stacking interactions of the Phe221 with the triazole and with the coumarinyl rings were also reported for the hit compound **1** as shown in Fig. 2 [13]. In addition, the Ser478 residue establishes a common H-bonding with the oxymethylene linker of compounds **2i**, **2d**, and **2b** as well as the hit compound **1** [13]. However, compound **2i** is the only one that could form direct H-bond interactions with both Thr310 and Ser478 residues (Fig. 4B), while that of the Ser478 was only observed for the others (**2d** and **2b**), Fig. 4C–D. This suggested that the direct H-bonding interaction with Thr310 residue may be responsible for a striking inhibitory effect of the most potent compound **2i**. Accordingly, it is suggested that further investigations are necessary to reveal insight mechanism of inhibition and kinetics of these novel compounds.

Non-steroidal aromatase inhibitors currently used in clinical such as letrozole and anastrozole are 1,2,4-triazole based compounds.

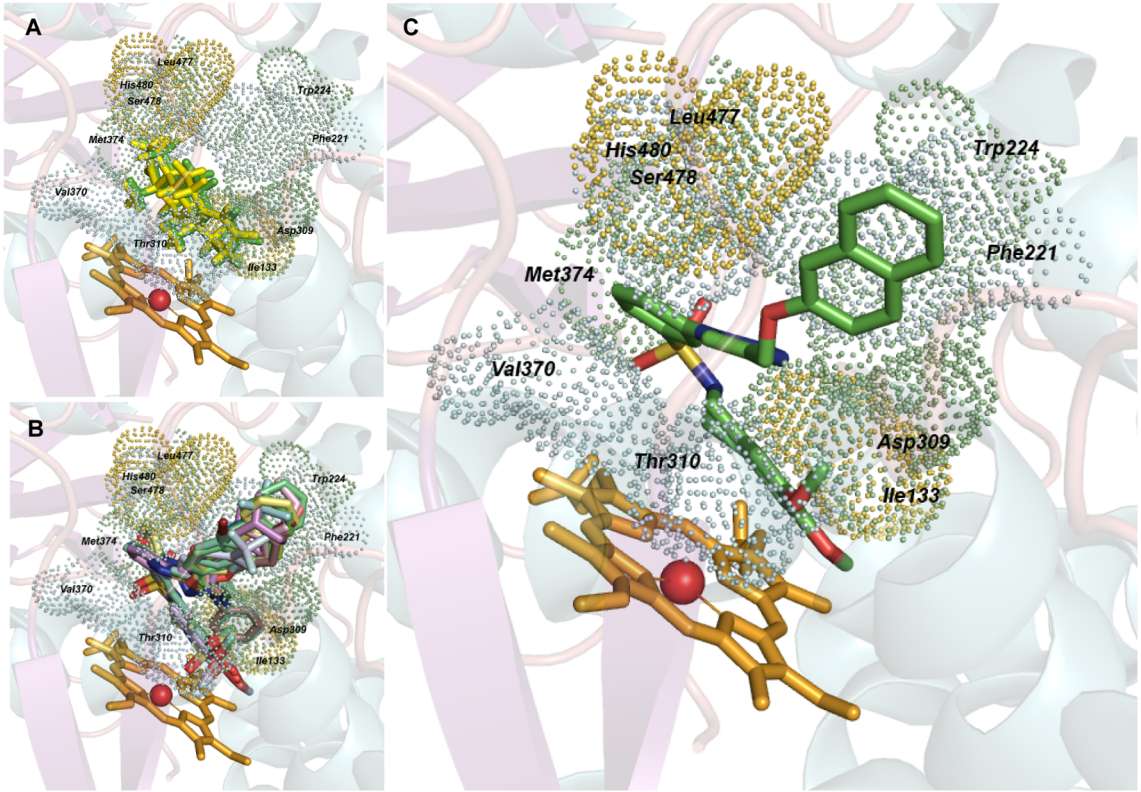

Fig. 3. Possible binding modalities of the investigated triazoles (heme and Fe atom of the aromatase enzyme active site are shown in orange and red, respectively, and key protein residues are presented as colored dotted); **(A)** Redocking of the natural substrate ASD providing RMSD = 0.705 A°. Docking pose of the original ASD is shown in yellow while those of the redocked ASD is shown in green; **(B)** Docking poses of thirteen investigated triazoles in the active site of aromatase enzyme; **(C)** The most potent compound **2i** occupying the enzyme active site.

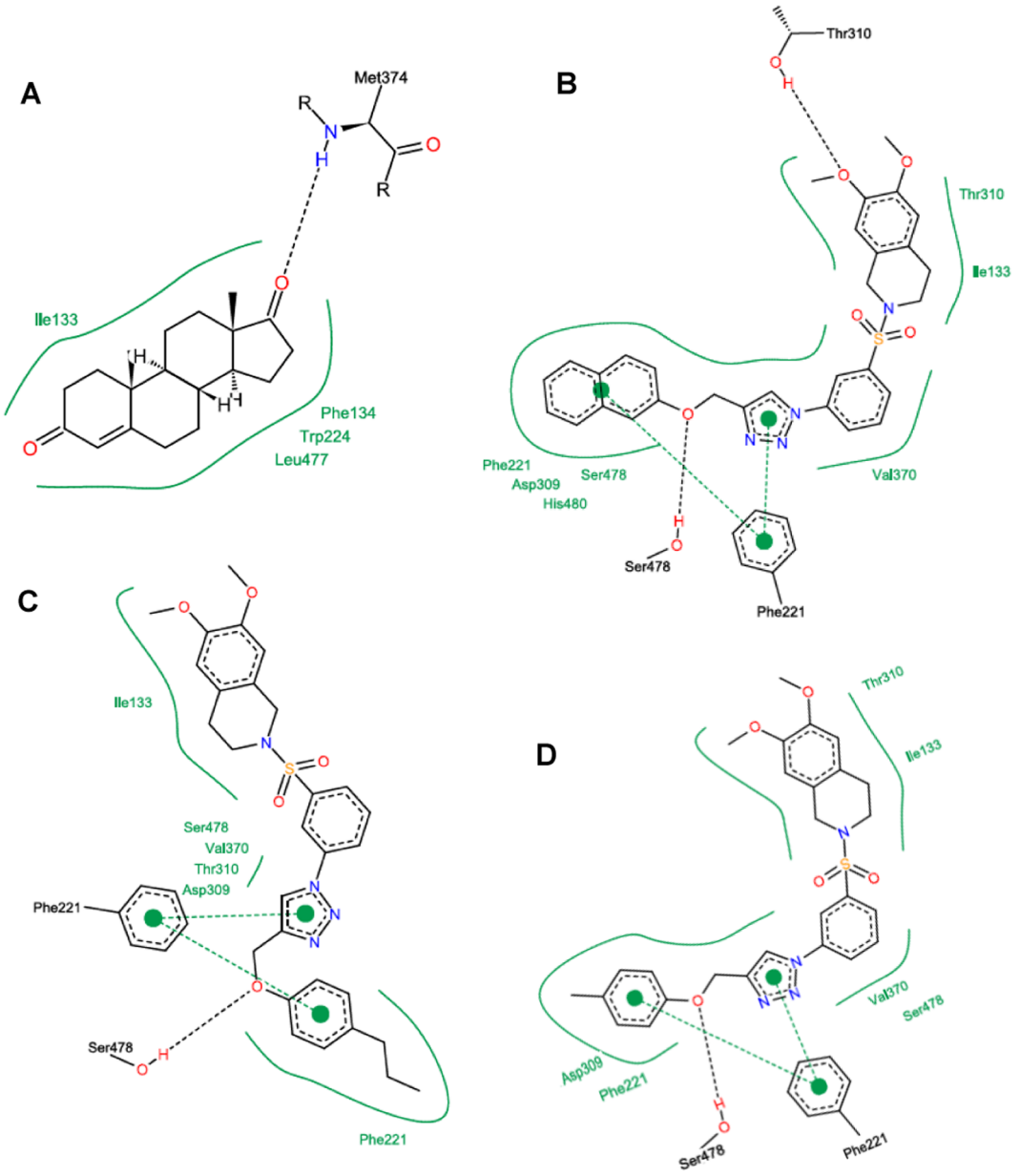

Fig. 4. The 2D ligand-protein interactions of natural substrate ASD* (A), compound **2i** (B), compound **2d** (C), and compound **2b** (D). *Additional hydrogen bond between Asp309 and carbonyl oxygen at C-3 of ASD has been reported (data not shown) [15].

However, the mechanism of aromatase inhibition of the triazoles is still controversial. Many possible mechanisms of inhibition have been proposed including competitive, non-competitive (allosteric), or mixed inhibition [23–25]. Molecular dynamic study revealed that the 1,2,4-triazole-based compounds could elicit aromatase inhibitory effect *via* competitive inhibition mechanism, in which a coordination interaction between nitrogen atom of the 1,2,4-triazole ring and the Fe atom of aromatase heme is considered a crucial interaction for the inhibitory activity [23].

Our molecular docking finding revealed that the investigated 1,2,3-triazole-based compounds (**2a-m)** could competitively bind in active site of the aromatase enzyme to elicit their inhibitory effects (Fig. 3), and was in agreement with the hypothesized competitive inhibition mechanism. However, the 2D ligand-protein interaction diagrams (Fig. 4) showed that these compounds interacted with the target aromatase enzyme *via* several types of interactions, except for the direct coordination with Fe atom of the aromatase heme.

Considering the competitive nature as well as limitations caused by long-term used of available steroidal and non-steroidal aromatase inhibitors [24], current attention has been given to the discovery of alternative non-competitive/allosteric aromatase inhibitors since an estrogen receptor modulator namely tamoxifen has been reported to inhibit aromatase enzyme activity *via* allosteric mechanism and its three potential allosteric pockets were noted [25]. This finding has led the searching for the inhibitors with alternative mode of inhibition. Previous kinetics study indicated that the letrozole, a 1,2,4-triazole containing drug, could act as a non-competitive or mixed aromatase inhibitor [26]. Allosteric inhibition of the letrozole was also confirmed by the work of Spinello et al. [27], which investigated the binding mode of letrozole against allosteric pockets [25] by performing molecular dynamics and free energy simulation.

Aromatase enzyme is a metalloprotein, which contains metal ions in its binding sites. The binding sites of metalloproteins are highly polarized due to the locating high coordinated-numbered metal ions. It is widely recognized that the molecular docking of metalloproteins is challenging due to multiple coordination geometries, lack of

sufficiently accurate force field parameters, and requirement of optimizing metal ion parameters [28]. Most of the current docking methods use force field based fixed electric charges for scoring electrostatic energy portion of both ligand and protein, in which the determined charges of metal ions may not appropriate for docking to provide preferable accuracy [29]. To overcome this limitation, it has been suggested that the protein atoms surrounding the binding sites together with the nearby metal ions should be included, in addition to the ligand atoms, as a part of quantum region for quantum mechanics/molecular mechanics (QM/MM) calculations in scoring function of molecular docking [29]. Several previous works demonstrated that, despite of extended time of calculation, using QM/MM docking could improve the accuracy of pose predictions [28,30,31].

Accordingly, further investigation using *in vitro* kinetic assay is recommended to elucidate actual mechanism of inhibition of these novel potential 1,2,3-triazole-based inhibitors. It is also suggested that further insight investigations using other computational methods (such as molecular dynamics) and softwares (which are be able for inclusion of water molecule and metal ion in the docking simulation) are required for overcoming the limitations of this study to provide more accurate definite binding modalities, interactions, and mechanisms of action of these compounds.

3. Conclusions

Thirteen tetrahydroisoquinoline-triazole hybrids (**2a-m**) have been achieved using the Pictet-Spengler and CuAAC reactions as the key steps. Their aromatase inhibitory activities and molecular docking were investigated. Seven triazoles exerted the aromatase inhibitory activity (IC_{50} = 0.07–1.9 μM) superior than that of the ketoconazole. Particularly, the triazole **2i** was shown to be the most potent inhibitor (IC_{50} = 0.07 μM) without affecting the non-cancerous cell line. Its inhibition potency was improved 3-fold compared with the hit compound **1**. The molecular docking also suggested that the formation of hydrogen bonding between the methoxy group of compound **2i** and the Thr310 residue of the enzyme may be essential for its highly potent aromatase inhibitory effect. In summary, a set of tetrahydroisoquinoline-triazole hybrids was highlighted as promising compounds to be further developed for managing estrogen-dependent diseases and cancers. The molecular docking results are also useful for guiding the design and synthesis of new aromatase inhibitors with improved potency and properties.

4. Experimental

4.1. General

Column chromatography was carried out using silica gel 60 (70–230 mesh ASTM). Analytical thin-layer chromatography (TLC) was performed with silica gel 60 F_{254} aluminum sheets. ^{1}H- and ^{13}C-NMR spectra were recorded on a Bruker AVANCE 300 and a Bruker Ascend^{TM} 400 NMR spectrometers. ^{1}H NMR and ^{13}C NMR chemical shifts are reported in ppm using tetramethylsilane (TMS) or residual non-deuterated solvent peak as an internal standard. The following standard abbreviations were used for signal multiplicities: singlet (s), doublet (d), triplet (t), quartet (q) and multiplet (m). FTIR spectra were obtained using a universal attenuated total reflectance attached on a Perkin–Elmer Spectrum One spectrometer. Mass spectra were recorded on a Bruker Daltonics (microTOF). Melting points were determined using a Griffin melting point apparatus and were uncorrected.

Compound **6** was prepared according to literature procedures [13]. All chemicals were used without further purification and purchased from commercial sources. A recombinant human aromatase (CYP19) and *O*-benzyl fluorescein benzyl ester (DBF) were supplied with the BD GentestTM kit from BD Biosciences-Discovery Labware (Woburn, USA). Reagents using in cell culture and assay were obtained from the following sources: DMEM (Dulbecco's Modified Eagle's Medium), RPMI-1640 (Rosewell Park Memorial Institute medium), FBS (fetal bovine serum) from Hyclone laboratories (Logan, UT, USA); MTT (3(4,5-dimethylthiazole-2-yl)-2,5-diphenyltetrazolium bromide), L-glutamine, penicillin-streptomycin, insulin and glucose from Sigma-Aldrich (St. Louis, MO, USA).

4.2. General procedure for the synthesis of alkynes (5a-i)

A propargyl bromide (12 mmol) was added to a suspension of an appropiate phenol **3a-i** (10 mmol) and potassium carbonate (15 mmol) in acetone (15 mL). The suspension was heated to reflux until completion of reaction (monitored by TLC). The reaction was allowed to cool and then concentrated under reduced pressure. Water (30 mL) was added and extracted with EtOAc (3 × 30 mL). The organic extracts were combined and washed with water (20 mL) and brine (20 mL). The organic layer was dried over anhydrous sodium sulfate, filtered and concentrated. The crude product was purified by column chromatography.

^{1}H NMR spectra of (prop-2-yn-1-yloxy)benzene (**5a**) [32], 1-methyl-4-(prop-2-yn-1-yloxy)benzene (**5b**) [32], 1-ethyl-4-(prop-2-yn-1-yloxy) benzene (**5c**) [33], 1-(*tert*-butyl)-4-(prop-2-yn-1-yloxy)benzene (**5e**) [33], 4-(prop-2-yn-1-yloxy)-1,1′-biphenyl (**5f**) [34], 1-bromo-4-(prop-2-yn-1-yloxy)benzene (**5 h**) [32], and 2-(prop-2-yn-1-yloxy)naphthalene (**5i**) [35] were consistent with those of the published result.

4.2.1. 1-(Prop-2-yn-1-yloxy)-4-propylbenzene (5d)

Pale yellow oil. 90% yield. ^{1}H NMR (300 MHz, $CDCl_3$) δ 0.91 (t, J = 7.3 Hz, 3H, CH_3), 1.59 (sext, J = 7.6 Hz, 2H, CH_2CH_3), 2.49 (t, J = 2.6 Hz, 1H, $HC{\equiv}C$), 2.52 (t, J = 7.4 Hz, 2H, CH_2Ar), 4.65 (s, 2H, CH_2O), 6.88 (d, J = 8.6 Hz, 2H, Ar*H*), 7.09 (d, J = 8.6 Hz, 2H, Ar*H*). ^{13}C NMR (75 MHz, $CDCl_3$) δ 13.8, 24.7, 37.2, 55.9, 75.3, 78.9, 114.7, 129.3, 135.8, 155.7.

4.2.2. 1-Benzyl-4-(prop-2-yn-1-yloxy)benzene (5g)

Pale yellow oil. 93% yield. ^{1}H NMR (300 MHz, $CDCl_3$) δ 2.52 (t, J = 2.5 Hz, 1H, $HC{\equiv}C$), 3.95 (s, 2H, CH_2Ar), 4.67 (s, 2H, CH_2O), 6.92 (d, J = 8.6 Hz, 2H, Ar*H*), 7.13 (d, J = 8.6 Hz, 2H, Ar*H*), 7.16–7.34 (m, 5H, Ar*H*). ^{13}C NMR (75 MHz, $CDCl_3$) δ 41.1, 55.9, 75.4, 78.8, 115.0, 126.0, 128.4, 128.9, 129.9, 134.3, 141.4, 156.0.

4.3. General procedure for the synthesis of alkynes (5j-k)

A propargyl bromide (12 mmol) was added to a suspension of an appropiate carboxylic acid **3j-k** (10 mmol) and potassium carbonate (15 mmol) in dimethylformamide (10 mL). The suspension was stirred at room temperature until completion of reaction (monitored by TLC). The reaction was allowed to cool and then concentrated under reduced pressure. Water (30 mL) was added and extracted with EtOAc (3 × 30 mL). The organic extracts were combined and washed with water (20 mL) and brine (20 mL). The organic layer was dried over anhydrous sodium sulfate, filtered and concentrated. The crude product was purified by column chromatography.

^{1}H NMR spectra of prop-2-yn-1-yl benzoate (**5j**) was consistent with that reported in the literature [36].

4.3.1. Prop-2-yn-1-yl adamantane-1-carboxylate (5k)

Pale yellow oil. 80% yield. ^{1}H NMR (300 MHz, $CDCl_3$) δ 1.69 (s, 6H, 3 × CH_2), 1.90 (s, 6H, 3 × CH_2), 2.00 (s, 3H, 3 × CH), 2.42 (t, J = 2.5 Hz, 1H, $HC{\equiv}C$), 4.62 (s, 2H, CH_2O). ^{13}C NMR (75 MHz, $CDCl_3$) δ 27.9, 36.6, 38.7, 40.7, 51.7, 74.4, 78.1, 176.8.

4.4. General procedure for the synthesis of triazoles (2a-m)

To a stirred solution of azide **6** (0.2 mmol) and the corresponding alkyne **5** (0.2 mmol) in *t*-BuOH:H_2O (3:3 mL), $CuSO_4{\cdot}5H_2O$ (0.2 mmol)

and ascorbic acid (0.5 mmol) were added. The reaction mixture was stirred at room temperature for 2–12 h (monitored by TLC), then concentrated under reduced pressure. The residue was added water (10 mL) and extracted with dichloromethane (3 × 20 mL). The combined organic phases were washed with water (20 mL), dried over anh. Na_2SO_4 and evaporated to dryness. The crude product was purified using silica gel column chromatography and eluted with methanol:dichloromethane (1:50).

*4.4.1. 6,7-Dimethoxy-2-((3-(4-(phenoxymethyl)-1H-1,2,3-triazol-1-yl) phenyl)sulfonyl)-1,2,3,4-tetrahydroisoquinoline (**2a**)*

White solid. 78% yield. mp 153–154 °C. IR (UATR) cm^{-1}: 1598, 1518, 1347, 1226, 1157, 1117. ^{1}H NMR (300 MHz, $CDCl_3$) δ 2.85 (t, J = 5.7 Hz, 2H, C4-THIQ*H*), 3.45 (t, J = 5.7 Hz, 2H, C3-THIQ*H*), 3.82 (s, 6H, 2 × OCH_3), 4.28 (s, 2H, C1-THIQ*H*), 5.32 (s, 2H, CH_2O), 6.53, 6.54 (2 s, 2H, Ar*H*), 6.97–7.07 (m, 3H, Ar*H*), 7.33 (t, J = 7.4 Hz, 2H, Ar*H*), 7.71 (t, J = 8.0 Hz, 1H, Ar*H*), 7.90 (d, J = 7.9 Hz, 1H, Ar*H*), 8.02 (d, J = 8.0 Hz, 1H, Ar*H*), 8.13 (s, 1H, C*H*N), 8.20 (s, 1H, Ar*H*). ^{13}C NMR (75 MHz, $CDCl_3$) δ 28.2, 43.9, 47.2, 55.9, 56.0, 61.9, 109.0, 111.4, 114.8, 119.3, 120.8, 121.5, 122.9, 124.4, 124.8, 127.5, 129.7, 130.8, 137.5, 139.2, 145.8, 147.9, 148.1, 158.1. HRMS-TOF: m/z $[M+Na]^+$ 529.1513 (Calcd for $C_{26}H_{26}N_4NaO_5S$: 529.1516).

*4.4.2. 6,7-Dimethoxy-2-((3-(4-((p-tolyloxy)methyl)-1H-1,2,3-triazol-1-yl)phenyl)sulfonyl)-1,2,3,4-tetrahydroisoquinoline (**2b**)*

White solid. 93% yield. mp 129–130 °C. IR (UATR) cm^{-1}: 1612, 1509, 1347, 1226, 1157, 1117. ^{1}H NMR (300 MHz, $CDCl_3$) δ 2.31 (s, 3H, CH_3), 2.85 (t, J = 5.7 Hz, 2H, C4-THIQ*H*), 3.45 (t, J = 5.7 Hz, 2H, C3-THIQ*H*), 3.82 (s, 6H, 2 × OCH_3), 4.28 (s, 2H, C1-THIQ*H*), 5.29 (s, 2H, CH_2O), 6.53, 6.55 (2 s, 2H, Ar*H*), 6.93 (d, J = 8.6 Hz, 2H, Ar*H*), 7.12 (d, J = 8.4 Hz, 2H, Ar*H*), 7.71 (t, J = 8.0 Hz, 1H, Ar*H*), 7.89 (d, J = 8.0 Hz, 1H, Ar*H*), 8.02 (dd, J = 8.0, 1.2 Hz, 1H, Ar*H*), 8.12 (s, 1H, C*H*N), 8.20 (t, J = 1.7 Hz, 1H, Ar*H*). ^{13}C NMR (75 MHz, $CDCl_3$) δ 20.5, 28.2, 43.9, 47.2, 55.9, 56.0, 62.0, 108.9, 111.4, 114.6, 119.3, 120.8, 122.9, 124.4, 124.8, 127.4, 130.1, 130.8, 130.9, 137.5, 139.2, 146.0, 147.9, 148.1, 156.0. HRMS-TOF: m/z $[M+Na]^+$ 543.1662 (Calcd for $C_{27}H_{28}N_4NaO_5S$: 543.1673).

*4.4.3. 2-((3-(4-((4-Ethylphenoxy)methyl)-1H-1,2,3-triazol-1-yl)phenyl) sulfonyl)-6,7-dimethoxy-1,2,3,4-tetrahydroisoquinoline (**2c**)*

White solid. 76% yield. mp 135–136 °C. IR (UATR) cm^{-1}: 1611, 1509, 1347, 1226, 1157, 1117. ^{1}H NMR (300 MHz, $CDCl_3$) δ 1.22 (t, J = 7.6 Hz, 3H, CH_3), 2.61 (q, J = 7.6 Hz, 2H, CH_2), 2.85 (t, J = 5.8 Hz, 2H, C4-THIQ*H*), 3.45 (t, J = 5.9 Hz, 2H, C3-THIQ*H*), 3.82 (s, 6H, 2 × OCH_3), 4.28 (s, 2H, C1-THIQ*H*), 5.30 (s, 2H, CH_2O), 6.53, 6.54 (2 s, 2H, Ar*H*), 6.95 (d, J = 8.6 Hz, 2H, Ar*H*), 7.15 (d, J = 8.5 Hz, 2H, Ar*H*), 7.71 (t, J = 8.0 Hz, 1H, Ar*H*), 7.89 (d, J = 7.9 Hz, 1H, Ar*H*), 8.02 (d, J = 8.0 Hz, 1H, Ar*H*), 8.12 (s, 1H, C*H*N), 8.20 (s, 1H, Ar*H*). ^{13}C NMR (75 MHz, $CDCl_3$) δ 15.8, 28.0, 28.2, 43.9, 47.2, 55.9, 56.0, 62.1, 109.0, 111.5, 114.7, 119.3, 120.7, 123.0, 124.3, 124.8, 127.4, 128.9, 130.8, 137.4, 137.5, 139.2, 146.0, 147.9, 148.1, 156.1. HRMS-TOF: m/z $[M+Na]^+$ 557.1813 (Calcd for $C_{28}H_{30}N_4NaO_5S$: 557.1829).

*4.4.4. 6,7-Dimethoxy-2-((3-(4-((4-propylphenoxy)methyl)-1H-1,2,3-triazol-1-yl)phenyl)sulfonyl)-1,2,3,4-tetrahydroisoquinoline (**2d**)*

White solid. 93% yield. mp 139–140 °C. IR (UATR) cm^{-1}: 1611, 1509, 1347, 1226, 1157, 1117. ^{1}H NMR (300 MHz, $CDCl_3$) δ 0.91 (t, J = 7.3 Hz, 3H, CH_3), 1.50–1.68 (m, 2H, CH_2), 2.52 (t, J = 7.6 Hz, 2H, CH_2), 2.83 (t, J = 5.7 Hz, 2H, C4-THIQ*H*), 3.42 (t, J = 5.9 Hz, 2H, C3-THIQ*H*), 3.79 (s, 6H, 2 × OCH_3), 4.26 (s, 2H, C1-THIQ*H*), 5.27 (s, 2H, CH_2O), 6.51, 6.52 (2 s, 2H, Ar*H*), 6.93 (d, J = 8.6 Hz, 2H, Ar*H*), 7.10 (d, J = 8.5 Hz, 2H, Ar*H*), 7.68 (t, J = 8.0 Hz, 1H, Ar*H*), 7.87 (d, J = 7.9 Hz, 1H, Ar*H*), 7.99 (dd, J = 8.0, 1.1 Hz, 1H, Ar*H*), 8.10 (s, 1H, C*H*N), 8.17 (s, 1H, Ar*H*). ^{13}C NMR (75 MHz, $CDCl_3$) δ 13.7, 24.7, 28.2, 37.1, 43.9, 47.2, 55.9, 56.0, 62.0, 109.0, 111.5, 114.6, 119.3, 120.8, 123.0, 124.3, 124.8, 127.4, 129.5, 130.8, 135.8, 137.5, 139.2, 146.0, 147.9, 148.1, 156.2. HRMS-TOF: m/z $[M+Na]^+$ 571.1989 (Calcd for $C_{29}H_{32}N_4NaO_5S$: 571.1986).

*4.4.5. 2-((3-(4-((4-(Tert-butyl)phenoxy)methyl)-1H-1,2,3-triazol-1-yl) phenyl)sulfonyl)-6,7-dimethoxy-1,2,3,4-tetrahydroisoquinoline (**2e**)*

White solid. 78% yield. mp 81–82 °C. IR (UATR) cm^{-1}: 1610, 1514, 1348, 1238, 1158, 1118. ^{1}H NMR (300 MHz, $CDCl_3$) δ 1.31 (s, 9H, 3 × CH_3), 2.85 (br t, 2H, C4-THIQ*H*), 3.45 (br t, J = 5.4 Hz, 2H, C3-THIQ*H*), 3.82 (s, 6H, 2 × OCH_3), 4.28 (s, 2H, C1-THIQ*H*), 5.31 (s, 2H, CH_2O), 6.53, 6.55 (2 s, 2H, Ar*H*), 6.97 (d, J = 8.8 Hz, 2H, Ar*H*), 7.34 (d, J = 8.7 Hz, 2H, Ar*H*), 7.71 (t, J = 8.0 Hz, 1H, Ar*H*), 7.89 (d, J = 7.8 Hz, 1H, Ar*H*), 8.02 (d, J = 8.1 Hz, 1H, Ar*H*), 8.13 (s, 1H, C*H*N), 8.20 (s, 1H, Ar*H*). ^{13}C NMR (75 MHz, $CDCl_3$) δ 28.2, 31.5, 34.1, 43.9, 47.2, 55.9, 56.0, 62.0, 109.0, 111.4, 114.2, 119.3, 120.8, 122.9, 124.4, 124.8, 126.4, 127.4, 130.8, 137.5, 139.2, 144.3, 146.0, 147.9, 148.1, 155.8. HRMS-TOF: m/z $[M+Na]^+$ 585.2127 (Calcd for $C_{30}H_{34}N_4NaO_5S$: 585.2142).

*4.4.6. 2-((3-(4-(([1,1′-Biphenyl]-4-yloxy)methyl)-1H-1,2,3-triazol-1-yl) phenyl)sulfonyl)-6,7-dimethoxy-1,2,3,4-tetrahydroisoquinoline (**2f**)*

White solid. 86% yield. mp 160–161 °C. IR (UATR) cm^{-1}: 1609, 1519, 1348, 1239, 1158, 1117. ^{1}H NMR (300 MHz, $CDCl_3$) δ 2.85 (t, J = 5.7 Hz, 2H, C4-THIQ*H*), 3.45 (t, J = 5.7 Hz, 2H, C3-THIQ*H*), 3.82 (s, 6H, 2 × OCH_3), 4.29 (s, 2H, C1-THIQ*H*), 5.37 (s, 2H, CH_2O), 6.53, 6.54 (2 s, 2H, Ar*H*), 7.11 (d, J = 8.8 Hz, 2H, Ar*H*), 7.32 (t, J = 7.4 Hz, 2H, Ar*H*), 7.43 (t, J = 7.5 Hz, 1H, Ar*H*), 7.52–7.60 (m, 4H, Ar*H*), 7.72 (t, J = 8.0 Hz, 1H, Ar*H*), 7.90 (d, J = 7.9 Hz, 1H, Ar*H*), 8.03 (d, J = 8.0 Hz, 1H, Ar*H*), 8.15 (s, 1H, C*H*N), 8.21 (s, 1H, Ar*H*). ^{13}C NMR (75 MHz, $CDCl_3$) δ 28.2, 43.9, 47.2, 55.9, 56.0, 62.0, 109.0, 111.4, 115.1, 119.3, 120.9, 122.9, 124.4, 124.8, 126.8, 126.9, 127.5, 128.3, 128.8, 130.8, 134.7, 137.5, 139.3, 140.6, 145.7, 147.9, 148.1, 157.6. HRMS-TOF: m/z $[M+Na]^+$ 605.1834 (Calcd for $C_{32}H_{30}N_4NaO_5S$: 605.1829).

*4.4.7. 2-((3-(4-((4-Benzylphenoxy)methyl)-1H-1,2,3-triazol-1-yl)phenyl) sulfonyl)-6,7-dimethoxy-1,2,3,4-tetrahydroisoquinoline (**2g**)*

White solid. 87% yield. mp 137–138 °C. IR (UATR) cm^{-1}: 1611, 1509, 1348, 1226, 1157, 1117. ^{1}H NMR (300 MHz, $CDCl_3$) δ 2.85 (t, J = 5.8 Hz, 2H, C4-THIQ*H*), 3.45 (t, J = 5.9 Hz, 2H, C3-THIQ*H*), 3.82 (s, 6H, 2 × OCH_3), 3.94 (s, 2H, CH_2Ph), 4.28 (s, 2H, C1-THIQ*H*), 5.29 (s, 2H, CH_2O), 6.53, 6.55 (2 s, 2H, Ar*H*), 6.96 (d, J = 8.6 Hz, 2H, Ar*H*), 7.10–7.32 (m, 7H, Ar*H*), 7.71 (t, J = 8.0 Hz, 1H, Ar*H*), 7.89 (d, J = 8.0 Hz, 1H, Ar*H*), 8.02 (d, J = 8.0 Hz, 1H, Ar*H*), 8.11 (s, 1H, C*H*N), 8.20 (s, 1H, Ar*H*). ^{13}C NMR (75 MHz, $CDCl_3$) δ 28.2, 41.1, 43.8, 47.2, 55.9, 56.0, 62.0, 109.0, 111.5, 114.8, 119.3, 120.8, 122.9, 124.3, 124.8, 126.1, 127.4, 128.5, 128.8, 130.0, 130.8, 134.3, 137.5, 139.2, 141.3, 145.9, 147.9, 148.1, 156.5. HRMS-TOF: m/z $[M+H]^+$ 597.2162 (Calcd for $C_{33}H_{33}N_4O_5S$: 597.2166).

*4.4.8. 2-((3-(4-((4-Bromophenoxy)methyl)-1H-1,2,3-triazol-1-yl)phenyl) sulfonyl)-6,7-dimethoxy-1,2,3,4-tetrahydroisoquinoline (**2h**)*

White solid. 91% yield. mp 73–74 °C. IR (UATR) cm^{-1}: 1600, 1489, 1344, 1244, 1157, 1119. ^{1}H NMR (300 MHz, $CDCl_3$) δ 2.85 (t, J = 5.8 Hz, 2H, C4-THIQ*H*), 3.45 (t, J = 5.8 Hz, 2H, C3-THIQ*H*), 3.82 (s, 6H, 2 × OCH_3), 4.29 (s, 2H, C1-THIQ*H*), 5.28 (s, 2H, CH_2O), 6.53, 6.54 (2 s, 2H, Ar*H*), 6.93 (d, J = 8.9 Hz, 2H, Ar*H*), 7.42 (d, J = 8.9 Hz, 1H, Ar*H*), 7.71 (t, J = 8.0 Hz, 1H, Ar*H*), 7.90 (d, J = 7.9 Hz, 1H, Ar*H*), 8.02 (d, J = 8.0 Hz, 1H, Ar*H*), 8.10 (s, 1H, C*H*N), 8.19 (s, 1H, Ar*H*). ^{13}C NMR (75 MHz, $CDCl_3$) δ 28.2, 43.8, 47.2, 55.9, 56.0, 62.1, 109.0, 111.5, 113.8, 116.6, 119.3, 120.9, 122.9, 124.4, 124.8, 127.5, 130.8, 132.5, 137.4, 139.4, 145.3, 147.9. 148.1, 157.2. HRMS-TOF: m/z $[M+Na]^+$ 607.0613 (Calcd for $C_{26}H_{25}BrN_4NaO_5S$: 607.0621).

*4.4.9. 6,7-Dimethoxy-2-((3-(4-((naphthalen-2-yloxy)methyl)-1H-1,2,3-triazol-1-yl)phenyl)sulfonyl)-1,2,3,4-tetrahydroisoquinoline (**2i**)*

White solid. 94% yield. mp 150–151 °C. IR (UATR) cm^{-1}: 1599,

1519, 1348, 1257, 1158, 1118. ^{1}H NMR (300 MHz, $CDCl_3$) δ 2.84 (t, J = 5.8 Hz, 2H, C4-THIQ*H*), 3.45 (t, J = 5.9 Hz, 2H, C3-THIQ*H*), 3.81 (s, 6H, 2 × OC*H*$_3$), 4.29 (s, 2H, C1-THIQ*H*), 5.44 (s, 2H, C*H*$_2$O), 6.53, 6.54 (2 s, 2H, Ar*H*), 7.20–7.50 (m, 4H, Ar*H*), 7.70 (t, J = 8.0 Hz, 1H, Ar*H*), 7.74–7.81 (m, 3H, Ar*H*), 7.89 (d, J = 7.9 Hz, 1H, Ar*H*), 8.02 (d, J = 8.1 Hz, 1H, Ar*H*), 8.16 (s, 1H, C*H*N), 8.21 (s, 1H, Ar*H*). ^{13}C NMR (75 MHz, $CDCl_3$) δ 28.2, 43.8, 47.2, 55.9, 56.0, 62.0, 107.4, 109.0, 111.5, 118.6, 119.4, 120.8, 123.0, 124.1, 124.3, 124.8, 126.6, 126.9, 127.4, 127.7, 129.3, 129.7, 130.8, 134.4, 137.5, 139.3, 145.7, 148.0, 148.1, 156.0. HRMS-TOF: m/z $[M+Na]^+$ 579.1670 (Calcd for $C_{30}H_{28}N_4NaO_5S$: 579.1673).

4.4.10. (1-(3-((6,7-Dimethoxy-3,4-dihydroisoquinolin-2(1H)-yl)sulfonyl) phenyl)-1H-1,2,3-triazol-4-yl)methyl benzoate (**2j**)

White solid. 87% yield. mp 75–76 °C. IR (UATR) cm^{-1}: 1717, 1600, 1519, 1451, 1348, 1268, 1157, 1116. ^{1}H NMR (400 MHz, $CDCl_3$) δ 2.85 (t, J = 5.6 Hz, 2H, C4-THIQ*H*), 3.44 (t, J = 5.7 Hz, 2H, C3-THIQ*H*), 3.82 (s, 6H, 2 × OC*H*$_3$), 4.27 (s, 2H, C1-THIQ*H*), 5.58 (s, 2H, C*H*$_2$O), 6.53, 6.54 (2 s, 2H, Ar*H*), 7.45 (t, J = 7.6 Hz, 2H, Ar*H*), 7.58 (t, J = 7.3 Hz, 1H, Ar*H*), 7.71 (t, J = 8.0 Hz, 1H, Ar*H*), 7.90 (d, J = 7.8 Hz, 1H, Ar*H*), 8.02 (d, J = 8.0 Hz, 1H, Ar*H*), 8.08 (d, J = 7.6 Hz, 2H, Ar*H*), 8.21 (s, 1H, Ar*H*), 8.22 (s, 1H, Ar*H*, C*H*N). ^{13}C NMR (100 MHz, $CDCl_3$) δ 28.2, 43.9, 47.2, 55.9, 57.9, 108.8, 111.3, 119.4, 122.3, 122.9, 124.4, 124.7, 127.6, 128.5, 129.5, 129.8, 130.8, 133.4, 137.4, 139.0, 144.3, 147.8, 148.0, 166.6. HRMS-TOF: m/z $[M+H]^+$ 535.1636 (Calcd for $C_{27}H_{27}N_4O_6S$: 535.1646).

4.4.11. (1-(3-((6,7-Dimethoxy-3,4-dihydroisoquinolin-2(1H)-yl)sulfonyl) phenyl)-1H-1,2,3-triazol-4-yl)methyl adamantane-1-carboxylate (**2k**)

White solid. 79% yield. mp 76–77 °C. IR (UATR) cm^{-1}: 1724, 1599, 1519, 1348, 1226, 1158, 1117. ^{1}H NMR (400 MHz, $CDCl_3$) δ 1.60–1.90 (m, 12H, 6 × C*H*$_2$), 1.99 (s, 3H, 3 × C*H*), 2.84 (t, J = 5.8 Hz, 2H, C4-THIQ*H*), 3.42 (t, J = 5.9 Hz, 2H, C3-THIQ*H*), 3.80 (s, 6H, 2 × OC*H*$_3$), 4.26 (s, 2H, C1-THIQ*H*), 5.27 (s, 2H, C*H*$_2$O), 6.52, 6.53 (2 s, 2H, Ar*H*), 7.70 (t, J = 8.0 Hz, 1H, Ar*H*), 7.87 (d, J = 7.9 Hz, 1H, Ar*H*), 7.99 (dd, J = 8.0, 1.2 Hz, 1H, Ar*H*), 8.19 (t, J = 1.7 Hz, 1H, Ar*H*), 8.20 (s, 1H, Ar*H*, C*H*N). ^{13}C NMR (100 MHz, $CDCl_3$) δ 27.8, 28.2, 36.4, 38.7, 40.7, 43.9, 47.2, 55.9, 56.0, 57.2, 108.8, 111.3, 119.4, 121.8, 122.8, 124.4, 124.7, 127.5, 130.8, 137.4, 139.0, 144.6, 147.8, 148.0, 177.6. HRMS-TOF: m/z $[M+Na]^+$ 615.2252 (Calcd for $C_{31}H_{36}N_4NaO_6S$: 615.2248).

4.4.12. 2-((3-(4-(4-Bromophenyl)-1H-1,2,3-triazol-1-yl)phenyl)sulfonyl)-6,7-dimethoxy-1,2,3,4-tetrahydroisoquinoline (**2l**)

White solid. 71% yield. mp 204–205 °C. IR (UATR) cm^{-1}: 1599, 1517, 1475, 1344, 1227, 1157, 1119. ^{1}H NMR (300 MHz, $CDCl_3$) δ 2.85 (t, J = 5.7 Hz, 2H, C4-THIQ*H*), 3.48 (t, J = 5.9 Hz, 2H, C3-THIQ*H*), 3.82 (s, 6H, 2 × OC*H*$_3$), 4.32 (s, 2H, C1-THIQ*H*), 6.53, 6.55 (2 s, 2H, Ar*H*), 7.62 (d, J = 8.5 Hz, 2H, Ar*H*), 7.74 (t, J = 8.0 Hz, 1H, Ar*H*), 7.80 (d, J = 8.5 Hz, 2H, Ar*H*), 7.92 (d, J = 7.9 Hz, 1H, Ar*H*), 8.08 (d, J = 8.1 Hz, 1H, Ar*H*), 8.21 (s, 1H, Ar*H*), 8.23 (s, 1H, C*H*N). ^{13}C NMR (75 MHz, $CDCl_3$) δ 28.1, 43.8. 47.3, 55.9, 56.0, 109.0, 111.5, 117.5, 119.2, 122.8, 122.9, 124.4, 124.8, 127.4, 128.7, 130.9, 132.2, 137.4, 138.6, 143.9, 147.9, 148.1 HRMS-TOF: m/z $[M+Na]^+$ 577.0513 (Calcd for $C_{25}H_{23}BrN_4NaO_4S$: 577.0516).

4.4.13. 6,7-Dimethoxy-2-((3-(4-(4-(trifluoromethyl)phenyl)-1H-1,2,3-triazol-1-yl)phenyl)sulfonyl)-1,2,3,4-tetrahydroisoquinoline (**2m**)

White solid. 70% yield. mp 159–160 °C. IR (UATR) cm^{-1}: 1622, 1516, 1484, 1324, 1228, 1158, 1120. ^{1}H NMR (300 MHz, $CDCl_3$) δ 2.84 (t, J = 5.7 Hz, 2H, C4-THIQ*H*), 3.49 (t, J = 5.9 Hz, 2H, C3-THIQ*H*), 3.81, 3.82 (2 s, 6H, 2 × OC*H*$_3$), 4.33 (s, 2H, C1-THIQ*H*), 6.54 (s, 2H, Ar*H*), 7.70–7.80 (m, 3H, Ar*H*), 7.94 (d, J = 7.9 Hz, 1H, Ar*H*), 8.02–8.13 (m, 3H, Ar*H*), 8.24 (s, 1H, Ar*H*), 8.32 (s, 1H, C*H*N). ^{13}C NMR (75 MHz, $CDCl_3$) δ 28.1, 43.8, 47.3, 55.9, 56.0, 108.4, 111.5, 118.3, 119.2, 122.9, 124.0 (q, $^1J_{CF}$ = 271 Hz), 124.4, 124.8, 126.0, 126.1, 127.6, 130.2 (q, $^2J_{CF}$ = 33 Hz), 130.9, 133.2, 137.4, 139.5, 147.6, 147.9, 148.1. HRMS-TOF: m/z $[M+Na]^+$ 567.1290 (Calcd for $C_{26}H_{23}F_3N_4NaO_4S$: 567.1284).

4.5. Aromatase inhibition assay

Aromatase inhibitory effect was performed using the method reported by Stressor et al. [37] with minor modification [13,38]. This method was carried out according to the Gentest kit using CYP19 enzyme and DBF as a fluorometric substrate. DBF was dealkylated by aromatase and then hydrolyzed to give the fluorescein product.

Briefly, 100 µL of cofactor, containing 78.4 µL of 50 mM phosphate buffer (pH 7.4); 20 µL of 20× NADPH-generating system (26 mM $NADP^+$, 66 mM glucose-6-phosphate, and 66 mM $MgCl_2$); and 1.6 µL of 100 U/mL glucose-6-phosphate dehydrogenase, was pipetted into a 96-well plate and preincubated in 37 °C (water bath) for 10 min. The reaction was initiated by addition of 100 µL of enzyme/substrate mixture containing 77.3 µL of 50 mM phosphate buffer (pH 7.4); 12.5 µL of 16 pmol/mL CYP19; 0.2 µL of 0.2 mM DBF, and 10 µL of 0.25 mM diluted tested sample or 10% DMSO as a negative control or letrozole/ketoconazole as a positive control. Fluorescence signal was recorded using an excitation wavelength of 490 nm and emission wavelength of 530 nm with cutoff 515 nm. Percentage of inhibition (% inhibition) was calculated as shown in Eq. (1). Samples with % inhibition greater than 50 were further diluted and assayed in triplicate. Finally, IC_{50} values were determined by plot of concentrations versus % inhibition.

$$\%\,inhibition = 100 - [(sample - blank)/(DMSO - blank) \times 100] \quad (1)$$

4.6. Cytotoxicity assay

The cytotoxic activity of compounds (**2a-m**) was tested using hormone-dependent breast cancer cell line (T47-D) and normal embryonic lung cell line (MRC-5). T47-D cells were grown in RPMI-1640 medium supplemented with 2 mM L-gluthamine, 100 U/mL penicillin-streptomycin, 0.2 U/mL insulin, 4.5 g/L glucose and 10% FBS whereas MRC-5 cells were grown in DMEM medium supplemented with 100 U/mL penicillin streptomycin and 10% FBS. Briefly, the cells suspended in the corresponding culture medium were inoculated in 96-well microtiter plates (Corning Inc., NY, USA) at a density of 10,000–20,000 cells per well, and then incubated at 37 °C under a humidified atmosphere with 95% air and 5% CO_2 for 24 h. An equal volume of additional medium containing either the serial dilutions of the tested compounds, positive control (etoposide and/or doxorubicin) or negative control (DMSO) was added to the desired final concentrations. The microtiter plates were further incubated for 48 h. Cell viability in each well was determined by staining with MTT assay [39–41]. The MTT solution (10 mL/100 mL medium) was added to all wells of the assay, and the plates were incubated for 2–4 h. Subsequently, DMSO was added to dissolve the resulting formazan by sonication. The plates were read on a microplate reader (Molecular Devices, USA) using a test wavelength of 550 nm and a reference wavelength of 650 nm. The IC_{50} value was determined as the compound concentration that inhibited cell growth by 50%. The compounds exhibited IC_{50} > 50 µg/mL were considered as non-cytotoxic.

4.7. Molecular docking

Molecular docking was performed to investigate possible binding modalities of the compounds (**2a-m**) toward the aromatase enzyme. Crystal structure of the target protein, human placental aromatase protein co-crystallized with natural substrate (ASD), was retrieved from RSCB protein data bank (PDB ID: 3EQM, http://www.rcsb.org/), and was prepared by adding essential hydrogen atoms and repairing missing side chains using the WHAT IF web server version 10.1 [42]. Subsequently, non-polar hydrogen atoms were merged, Gasteiger atomic charges were assigned, and atom type of the protein structures

were specified using AutoDock Tools version 1.5.6. [43,44]. All investigated triazole analogs (**2a-m**) were drawn using Marvin Sketch version 6.1.4 [45], and were geometrically optimized by Gaussian 09 [46] using Becke's three-parameter hybrid method with the Lee-Yang-Parr correlation functional (B3LYP) together with the 6-31 g(d) basis set. The structurally optimized compounds were prepared by merging non-polar hydrogen atoms, defining rotatable bonds and assigning partial atomic charge using AutoDock Tools version 1.5.6 [43,44]. AutoDock Vina, as a part of the PyRx 0.8 software [47], was used to perform the molecular docking simulation. Grid boxes size of 62.06 × 71.95 × 51.46 A° were generated and the center of binding cavity was allocated using x, y and z coordinates of 83.4375, 50.1006, and 46.3803, respectively. The co-crystallized ligand, ASD, was re-docked to the aromatase proteins as to validate docking protocol. The re-docking results were evaluated by calculation of root mean standard deviation (RMSD) using Chimera software [48]. Docking poses of the investigated compounds were visualized using PyMOL [49], and two-dimensional ligand-protein interaction diagrams were generated using PoseView (http://proteins.plus) [50].

Acknowledgments

This project is financially supported by Srinakharinwirot University (grant no. 012/2562). We gratefully acknowledge the support from the annual budget grant (BE 2562-2563) of Mahidol University. We are also indebted to Chulabhorn Research Institute for recording mass spectra and bioactivity testings.

Appendix A. Supplementary material

Supplementary data to this article can be found online at https://doi.org/10.1016/j.bioorg.2019.103327.

References

[1] C. Palmieri, D.K. Patten, A. Januszewski, G. Zucchini, S.J. Howell, Breast cancer: current and future endocrine therapies, Mol. Cell. Endocrinol. 382 (2014) 695–723.
[2] D. Ghosh, J. Lo, C. Egbuta, Recent progress in the discovery of next generation inhibitors of aromatase from the structure – function perspective, J. Med. Chem. 59 (2016) 5131–5148.
[3] I. Ahmad, Shagufta, Recent developments in steroidal and nonsteroidal aromatase inhibitors for the chemoprevention of estrogen-dependent breast cancer, Eur. J. Med. Chem. 102 (2015) 375–386.
[4] M.R. Yadav, M.A. Barmade, R.S. Tamboli, P.R. Murumkar, Developing steroidal aromatase inhibitors-an effective armament to win the battle against breast cancer, Eur. J. Med. Chem. 105 (2015) 1–38.
[5] N. Adhikari, S.A. Amin, A. Saha, T. Jha, Combating breast cancer with non-steroidal aromatase inhibitors (NSAIs): Understanding the chemico-biological interactions through comparative SAR/QSAR study, Eur. J. Med. Chem. 137 (2017) 365–438.
[6] F. Caporuscio, G. Rastelli, C. Imbriano, A. Del Rio, Structure-based design of potent aromatase inhibitors by high-throughput docking, J. Med. Chem. 54 (2011) 4006–4017.
[7] S. Gobbi, A. Rampa, F. Belluti, A. Bisi, Nonsteroidal aromatase inhibitors for the treatment of breast cancer: an update, Anticancer Agents Med. Chem. 14 (2014) 54–65.
[8] P.E. Lonning, H.P. Eikesdal, Aromatase inhibition clinical state of the art and questions that remain to be solved, Endocr. Relat. Cancer 20 (2013) (2013) R183–R201.
[9] A.F. Sobral, C. Amaral, G. Correia-da-Silva, N. Teixeira, Unravelling exemestane: from biology to clinical prospects, J. Steroid Biochem. Mol. Biol. 163 (2016) 1–11.
[10] A. Coates, A. Keshaviah, B. Thürlimann, H. Mouridsen, L. Mauriac, J.F. Forbes, R. Paridaens, M. Castiglione-Gertsch, R.D. Gelber, M. Colleoni, I. Láng, L. Del Mastro, I. Smith, J. Chirgwin, J.M. Nogaret, T. Pienkowski, A. Wardley, E.H. Jakobsen, K.N. Price, A. Goldhirsch, Five years of letrozole compared with tamoxifen as initial adjuvant therapy for postmenopausal women with endocrine-responsive early breast cancer: update of study BIG 1–98, J. Clin. Oncol. 25 (2007) 486–492.
[11] W. Amir, B. Seruga, S. Niraula, L. Carlsson, A. Ocaña, Toxicity of adjuvant endocrine therapy in postmenopausal breast cancer patients: A systematic review and meta-analysis, J. Natl. Cancer Inst. 103 (2011) 1299–1309.
[12] R. Sainsbury, The development of endocrine therapy for women with breast cancer, Cancer Treat. Rev. 39 (2013) 507–517.
[13] R. Pingaew, V. Prachayasittikul, P. Mandi, C. Nantasenamat, S. Prachayasittikul, S. Ruchirawat, V. Prachayasittikul, Synthesis and molecular docking of 1,2,3-triazole-based sulfonamides as aromatase inhibitors, Bioorg. Med. Chem. 23 (2015) 3472–3480.
[14] R. Leechaisit, R. Pingaew, V. Prachayasittikul, A. Worachartcheewan, S. Prachayasittikul, S. Ruchirawat, V. Prachayasittikul, Synthesis, molecular docking, and QSAR study of bis-sulfonamide derivatives as potential aromatase inhibitors, Bioorg. Med. Chem. (2019), https://doi.org/10.1016/j.bmc.2019.08.001.
[15] D. Ghosh, J. Griswold, M. Erman, W. Pangborn, Structural basis for androgen specificity and oestrogen synthesis in human aromatase, Nature 457 (2009) 219–223.
[16] G.P. Skliris, E. Leygue, P.H. Watson, L.C. Murphy, Estrogen receptor alpha negative breast cancer patients: Estrogen receptor beta as a therapeutic target, J. Steroid Biochem. Mol. Biol. 109 (2008) 1–10.
[17] T.M. Penning, M.C. Byrns, Steroid hormone transforming aldo-keto reductases and cancer, Ann. N. Y. Acad. Sci. 1155 (2009) 33–42.
[18] S. Endo, D. Hu, T. Matsunaga, Y. Otsuji, O. El-Kabbani, M. Kandeel, A. Ikari, A. Hara, Y. Kitade, N. Toyooka, Synthesis of non-prenyl analogues of baccharin as selective and potent inhibitors for aldo-keto reductase 1C3, Bioorg. Med. Chem. 22 (2014) 5220–5233.
[19] M.P. Thomas, B.V.L. Potter, Discovery and development of the aryl *O*-sulfamate pharmacophore for oncology and womens health, J. Med. Chem. 58 (2015) 7634–7658.
[20] K.M. McNamara, H. Sasano, The intracrinology of breast cancer, J. Steroid Biochem. Mol. Biol. 145 (2015) 172–178.
[21] K.E. Hevener, W. Zhao, D.M. Ball, K. Babaoglu, J. Qi, S.W. White, R.E. Lee, Validation of molecular docking programs for virtual screening against dihydropteroate synthase, J. Chem. Inf. Model. 49 (2009) 444–460.
[22] J.C. Cole, C.W. Murray, J.W. Nissink, R.D. Taylor, R. Taylor, Comparing protein-ligand docking programs is difficult, Proteins 60 (2005) 325–332.
[23] A. Mojaddami, A. Sakhteman, M. Fereidoonnezhad, Z. Faghih, A. Najdian, S. Khabnadideh, H. Sadeghpour, Z. Rezaei, Binding mode of triazole derivatives as aromatase inhibitors based on docking, protein ligand interaction fingerprinting, and molecular dynamics simulation studies, Res. Pharm. Sci. 12 (2017) 21–30.
[24] M.M.D.S. Cepa, E.J. Tavares da Silva, G. Correia-da-Silva, F.M.F. Roleira, N.A.A. Teixeira, Synthesis and biochemical studies of 17-substituted androst-3-enes and 3,4-epoxyandrostanes as aromatase inhibitors, Steroids. 73 (2008) 1409–1415.
[25] J. Sgrignani, M. Bon, G. Colombo, A. Magistrato, Computational approaches elucidate the allosteric mechanism of human aromatase inhibition: a novel possible route to small-molecule regulation of CYP450s activities? J. Chem. Inf. Model. 54 (2014) 2856–2868.
[26] C. Egbuta, J. Lo, D. Ghosh, Mechanism of inhibition of estrogen biosynthesis by azole fungicides, Endocrinology 155 (2014) 4622–4628.
[27] A. Spinello, S. Martini, F. Berti, M. Pennati, M. Pavlin, J. Sgrignani, G. Grazioso, G. Colombo, N. Zaffaroni, A. Magistrato, Rational design of allosteric modulators of the aromatase enzyme: An unprecedented therapeutic strategy to fight breast cancer, Eur. J. Med. Chem. 168 (2019) 253–262.
[28] A. Khandelwal, V. Lukacova, D. Comez, D.M. Kroll, S. Raha, S. Balaz, A combination of docking, QM/MM methods, and MD simulation for binding affinity estimation of metalloprotein ligands, J. Med. Chem. 48 (2005) 5437–5447.
[29] A.E. Cho, D. Rinaldo, Extension of QM/MM docking and its applications to metalloproteins, J. Comput. Chem. 30 (2009) 2609–2616.
[30] P. Chaskar, V. Zoete, U.F. Röhrig, On-the-Fly QM/MM docking with attracting cavities, J. Chem. Inf. Model. 57 (2017) 73–84.
[31] A.E. Cho, V. Guallar, B.J. Berne, R. Friesner, Importance of accurate charges in molecular docking: quantum mechanical/molecular mechanical (QM/MM) approach, J. Comput. Chem. 26 (2005) 915–931.
[32] C. Efe, I.N. Lykakis, M. Stratakis, Gold nanoparticles supported on TiO_2 catalyse the cycloisomerisation/oxidative dimerisation of aryl propargyl ethers, Chem. Commun. 47 (2011) 803–805.
[33] Y. Wu, M. Pan, Y. Dai, B. Liu, J. Cui, W. Shi, Q. Qiu, W. Huang, H. Qian, Design, synthesis and biological evaluation of LBM-A5 derivatives as potent P-glycoprotein-mediated multidrug resistance inhibitors, Bioorg. Med. Chem. 24 (2016) 2287–2297.
[34] G. Pintér, G. Batta, S. Kéki, A. Mándi, I. Komáromi, K. Takács-Novák, F. Sztaricskai, E. Roth, E. Ostorházi, F. Rozgonyi, L. Naesens, P. Herczegh, Diazo transfer-click reaction route to new, lipophilic teicoplanin and ristocetin aglycon derivatives with high antibacterial and anti-influenza virus activity: an aggregation and receptor binding study, J. Med. Chem. 52 (2009) 6053–6061.
[35] Y. Tsuzuki, T.K.N. Nguyen, D.R. Garud, B. Kuberan, M. Koketsu, 4-Deoxy-4-fluoro-xyloside derivatives as inhibitors of glycosaminoglycan biosynthesis, Bioorg. Med. Chem. Lett. 20 (2010) 7269–7273.
[36] I. Ott, K. Schmidt, B. Kircher, P. Schumacher, T. Wiglenda, R. Gust, Antitumor-active cobalt-alkyne complexes derived from acetylsalicylic acid: studies on the mode of drug action, J. Med. Chem. 48 (2005) 622–629.
[37] D.M. Stresser, S.D. Turner, J. McNamara, P. Stocker, V.P. Miller, C.L. Crespi, C.J. Patten, A high-throughput screen to identify inhibitors of aromatase (CYP19), Anal. Biochem. 284 (2000) 427–430.
[38] V. Prachayasittikul, R. Pingaew, A. Worachartcheewan, S. Sitthimonchai, C. Nantasenamat, S. Prachayasittikul, S. Ruchirawat, V. Prachayasittikul, Aromatase inhibitory activity of 1,4-naphthoquinone derivatives and QSAR study, EXCLI J. 16 (2017) 714–726.
[39] T. Mosmann, Rapid colorimetric assay for cellular growth and survival: application to proliferation and cytotoxicity assays, J. Immunol. Methods 65 (1983) 55–63.
[40] H. Tominaga, M. Ishiyama, F. Ohseto, K. Sasamoto, T. Hamamoto, K. Suzuki, M. Watanabe, A water-soluble tetrazolium salt useful for colorimetric cell viability assay, Anal. Commun. 36 (1999) 47–50.
[41] J. Carmichael, W.G. DeGraff, A.F. Gazdar, J.D. Minna, J.B. Mitchell, Evaluation of a

tetrazolium-based semiautomated colorimetric assay: assessment of radiosensitivity, Cancer Res. 47 (1987) 943–946.
[42] G. Vriend, WHAT IF: A molecular modeling and drug design program, J. Mol. Graph. 8 (1990) 52–56.
[43] M.F. Sanner, Python: a programming language for software integration and development, J. Mol. Graph. Model. 17 (1999) 57–61.
[44] G.M. Morris, R. Huey, W. Lindstrom, M.F. Sanner, R.K. Belew, D.S. Goodsell, A.J. Olson, AutoDock4 and AutoDockTools4: Automated docking with selective receptor flexibility, J. Comput. Chem. 30 (2009) 2785–2791.
[45] ChemAxon, Marvin Sketch Version 6.0, in, Budapest, Hungary, 2013.
[46] M.J. Frisch, G.W. Trucks, H.B. Schlegel, G.E. Scuseria, M.A. Robb, J.R. Cheeseman, G. Scalmani, V. Barone, B. Mennucci, G.A. Petersson, H. Nakatsuji, M. Caricato, X. Li, H.P. Hratchian, A.F. Izmaylov, J. Bloino, G. Zheng, J.L. Sonnenberg, M. Hada, M. Ehara, K. Toyota, R. Fukuda, J. Hasegawa, M. Ishida, T. Nakajima, Y. Honda, O. Kitao, H. Nakai, T. Vreven, J.A.M. Jr., J.E. Peralta, F. Ogliaro, M. Bearpark, J.J. Heyd, E. Brothers, K.N. Kudin, V.N. Staroverov, R. Kobayashi, J. Normand, K. Raghavachari, A. Rendell, J.C. Burant, S.S. Iyengar, J. Tomasi, M. Cossi, N. Rega, J. M. Millam, M. Klene, J.E. Knox, J.B. Cross, V. Bakken, C. Adamo, J. Jaramillo, R. Gomperts, R.E. Stratmann, O. Yazyev, A.J. Austin, R. Cammi, C. Pomelli, J.W. Ochterski, R.L. Martin, K. Morokuma, V.G. Zakrzewski, G.A. Voth, P. Salvador, J.J. Dannenberg, S. Dapprich, A.D. Daniels, Ö. Farkas, J.B. Foresman, J.V. Ortiz, J. Cioslowski, D.J. Fox, in, Gaussian Inc., Wallingford CT, 2009.
[47] S. Dallakyan, PyRx Version 0.8, in, http://pyrx.scripps.edu, 2013.
[48] E.F. Pettersen, T.D. Goddard, C.C. Huang, G.S. Couch, D.M. Greenblatt, E.C. Meng, T.E. Ferrin, UCSF Chimera–a visualization system for exploratory research and analysis, J. Comput. Chem. 25 (2004) 1605–1612.
[49] W. Delano, PyMOL Release 0.99, DeLano Scientific LLC, Pala Alto, Ca, 2002.
[50] R. Fährrolfes, S. Bietz, F. Flachsenberg, A. Meyder, E. Nittinger, T. Otto, A. Volkamer, M. Rarey, ProteinsPlus: a web portal for structure analysis of macromolecules, Nucleic Acids Res. 45 (2017) W337–W343.